Hindawi
Advances in Materials Science and Engineering
Volume 2021, Article ID 6624704, 12 pages
https://doi.org/10.1155/2021/6624704

Research Article

Effect of Ultrasonic Frequency on Thickener Performance

Gongcheng Li,[1] **Shulong Liu**,[2] **Zengsheng Wen**,[3] **Guolei Liu**,[1] **Yu Cui**,[1] **and Yajian Shao**[4]

[1]*School of Resources and Environmental Engineering, Shandong University of Technology, Zibo 255049, China*
[2]*School of Materials Science and Engineering, Shandong University of Technology, Zibo 255049, China*
[3]*Shandong Hualian Mining Co. Ltd, Zibo 256100, China*
[4]*School of Civil and Environmental Engineering, University of Science and Technology Beijing, Beijing 100083, China*

Correspondence should be addressed to Gongcheng Li; ligongcheng888@126.com and Shulong Liu; 1561593036@qq.com

Received 13 November 2020; Accepted 20 July 2021; Published 29 July 2021

Academic Editor: Guoqiang Xie

Gravity thickening is an important aspect to solve numerous environmental and safety problems that were created by tailings discharging at low solid concentrations. Furthermore, in order to efficiently facilitate the separation of released water and solid sediments, a continuous thickening system with ultrasonic equipment has been used to investigate the thickening performance of copper-mine tailings under different ultrasonic frequencies (16 kHz, 20 kHz, 22 kHz, 25 kHz, and 28 kHz). After freeze-drying treatment, the underflow samples are imaged using the scanning electron microscope (SEM); then, the structure of floc or aggregates in the SEM images is quantifiably analyzed using the software of Image J. Results show that the underflow concentration increases as the ultrasonic frequency increases and decreases afterwards. A linear logarithmic function can explain the relationship between underflow concentration and run time at a certain ultrasonic. The underflow concentration is maximized at 64.47 wt. % when the ultrasonic frequency is 22 kHz. Based on the analysis on the microstructure of underflow samples, the minimum pore average size and pore average fraction are obtained when the ultrasonic frequency is 22 kHz, implying that 22 kHz is the optimum ultrasonic frequency combining the results of the underflow concentration.

1. Introduction

Traditional tailings discharge at low solid concentrations can cause serious environmental pollution and disasters, including tailings dam failures and collapse of underground voids [1]. Cement paste backfill (CPB) [2] is considered as one of the green mining technologies to minimize the effect of mining activities, and the traditional tailings discharge will progressively be replaced by CPB which consists of mine tailings, binder, and water and are approximately 70–80 wt. % solids [2–5]. The solid components of CPB are mainly composed of gravity thickener outputs, which are usually produced in the thickening process. Tailings slurry thickening, which involves flocculation, solid-liquid separation under gravity, and low rate shearing, is a complicated process for paste production.

The aim of gravity thickening processes is to increase the solids concentration of particulate slurries [6]. Operationally, the tailings slurry and flocculant solution are fed to a gravity thickener via a feed well where they mix to produce flocculated aggregates or flocs. The flocs settle due to the solid-liquid density difference and are discharged as thickened underflow [7]. The aggregate structure is highly relevant with underflow concentration, and the rake remarkably improved the thickening performance by releasing trapped water in the thickening process. Owen et al. [8] showed that the rake may break the honeycomb structure of aggregates under low shear in the compression zone, and the intensity and duration of the rake action were critical factors. Many researchers [6, 9–13] concluded that the shear stress introduced by raking can dramatically improve the thickener performance in bed density, but it is still not enough to release an amount of water trapped in aggregates. However, at a business unit of Rio Tinto, a 2 wt. % improvement of the thickener underflow concentration would reduce the operating costs by millions of dollars annually [14]. In view of this, the ultrasonic energy of 2.01 (W/L) was applied to improve bed density in batch tests with a small cylinder

(400 mm height), and the results showed that the ultrasonic energy can adjust arrangement of flocs or particles and the bed density can be improved by 4.24 wt. % [14]. Onal et al. [15] also showed that, as a form of mechanical vibratory, ultrasound generates high compression and rarefaction forces that can break the surface tension and promote the separation of liquids from solids.

However, no significant studies reported for the application of the different ultrasonic frequencies on thickening performance in continuous tests. In this study, the raked continuous thickening laboratory system with ultrasonic equipment was used to obtain dewatering results (e.g., bed height and underflow concentration), and the effect of different ultrasonic frequencies on thickening performance was analyzed. Moreover, the microstructure is the intrinsic manifestation of macroscopic properties, and the microstructure of the aggregates and flocs in most research studies has been damaged greatly, and the results caused a large error. In this study, to stabilize the primary structure of aggregates and flocs, the freeze-drying method was used to pretreat the underflow samples, and then, the aggregate and floc structures were imaged by the scanning electron microscope (SEM). The changes in aggregate structures at different ultrasonic frequencies were analyzed statistically.

2. Materials and Methods

2.1. Tailings. The specific gravity of the unclassified tailings in Jiashi Copper Mine is 2.66. Different particle distributions of the unclassified tailings were determined using a He-Ne laser particle size analyzer (LS-POP(9)). Methods and parameters used for laser diffractometer experiments are shown in Table 1.

Physical properties of the tailings are described in Figure 1 and Table 2. The unclassified tailings can be considered as superfine tailings since 64.32% of the particles were smaller than 0.074 mm [16].

Figure 2 shows main mineral compositions of tailings mineralogy using XRD. SiO_2 was the main mineral within the tailings. The other important minerals were aluminosilicate-bearing minerals, magnesium-bearing silicate minerals, and $CaCO_3$.

Equations (1) and (2) are utilized for calculating the values of the uniformity coefficient (Cu) and curvature coefficient (Cc), which can be used to characterize the uniformity of particle size compositions that were provided. The size distribution of tailing particles is usually wide, and tailing is well graded when $Cu \geq 5$. Cc reflects the continuous gradation of tailings; tailings exhibit good gradation and a high compaction rate when $Cc = 1$–3 [17, 18]

$$C_U = \frac{d_{60}}{d_{10}}, \tag{1}$$

$$C_C = \frac{d_{30}^2}{d_{10} \times d_{60}}. \tag{2}$$

In accordance with Figure 1 and Table 1, the size distribution of Jiashi Copper Mine tailings is wide, and these tailings are well graded given that their Cu and Cc values are 18.88 and 1.59, respectively.

2.2. Feed Suspension Preparation. An overhead stirrer and a cross-blade impeller (120 mm length, 80 mm width, and 30 mm thickness) were used to mix and blend the unclassified tailings and tap water in a vessel for 24 hours at 300 rpm; to ensure adequate mixing and to obtain a homogenous mixture, the impeller was positioned less than 5 cm from the bottom of the vessel, and suspensions or slurries were produced at an initial concentration of 30 wt. %.

The polymer used was an anionic polyacrylamide flocculant, Magnafloc 5250, which was provided by Basf (Beijing) Pty. Ltd with an ultrahigh molecular weight of 12 million. The pH of the polymer is around 7, and 98% of the particles are smaller than 1000 μm [19, 20]. Two steps were required to prepare the solution of flocculant: (1) a stock solution of flocculant (0.1 wt. %) was prepared in tap water and rotated in a beaker at 240 rpm over 2 hours; (2) the solution was diluted with tap water into 0.01 wt. % working solution and blended in a beaker at 260 rpm over 2 hours.

2.3. Testing Devices and Methods

2.3.1. Continuous Thickening Tests. A schematic of the continuous thickening system is shown in Figure 3. The diameter of the acrylic settling column is 100 mm, which can be considered sufficient to minimize wall effect, and the height of the column is 1000 mm. The steel raked apparatus consisted of vertical pickets, and each rake comprised four vertical prongs (each of 10 mm diameter and 1100 mm length) welded to a horizontal arm. The separation distance between the prongs was 20 mm. The rakes were driven at the desired rotation of 4 rpm via a LWX 70 overhead motor. Feed slurry was flocculated in a pipe reactor of internal diameter 12.5 mm. The feed slurry was supplied at 0.6 L·min^{-1} via a MASTERFLEX 77200-62 peristaltic pump, and the solution of flocculant was pumped at 0.01 L·min^{-1} with the polymer of 30 g t^{-1} of tailings solids. The flocculated suspension was introduced at the top of the settling column with 1 mm increments along the side, starting the underflow pump with the brand being MASTERFLEX 77601-10 when the bed height was over 650 mm, and steady-state conditions were achieved from the stability of the bed height between 650 mm and 680 mm, and from a comparison of the solids removal rate versus the feed rate, this process is to stimulate the running of thickeners. The height of the solid-liquid interface was marked by hands and monitored by a Streamview FR-200 high-definition video camera which was connected to a computer for a period of 1.5 h. Approximately 20 cm^3 of underflow samples were obtained from the sampling point via the lowest sampling valve with distance being 100 mm from the base of the column at steady-state conditions (the bed heights were stable), and the solids concentration were determined using the oven drying method, and the steps were taken as follows:

Table 1: Methods and parameters used for laser diffractometer experiments.

Method	Dispersant	Refractive index	Absorption factor	Measurement time (s)	Number of repetitions	Standard deviation
Wet measurement	Water	2.4	0.1	20	3	1.45

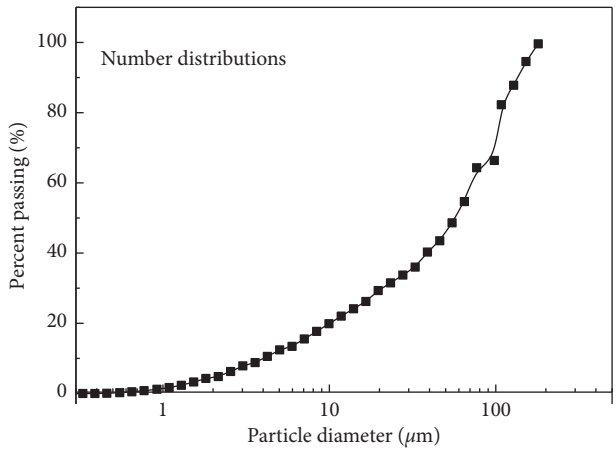

Figure 1: Particle size distributions of the utilized tailings.

Table 2: Physical parameters of the utilized tailings.

Element	D_{10} (mm)	D_{30} (mm)	D_{50} (mm)	D_{60} (mm)	D_{90} (mm)	G_s	C_u	C_c
Tailings	4.24×10^{-3}	23.25×10^{-3}	54.74×10^{-3}	80.05×10^{-3}	132.19×10^{-3}	2.58	18.88	1.59

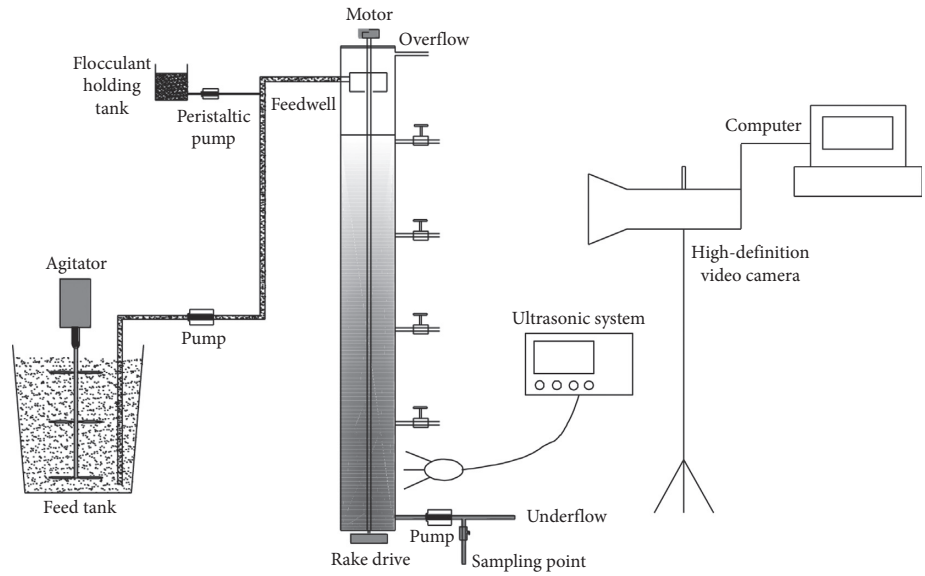

Figure 2: Schematic of the continuous thickening laboratory system.

(1) Take a known weight container to obtain the underflow samples; then, weigh the moist samples

(2) Dry the samples in an oven at a temperature of 105°C for 24 hours

(3) Weigh the samples and determine the moisture loss by subtracting the oven dry weight from the moist weight

(4) Calculate the solid concentration of underflow samples

A wave from the ultrasonic system is a kind of sonic wave, with frequency from 16 to 28 kHz and a power of 200 W; to generate sonic waves with different frequencies, each frequency has its transducer. The experiments mainly focus on the effect of ultrasonic frequencies on the thickener

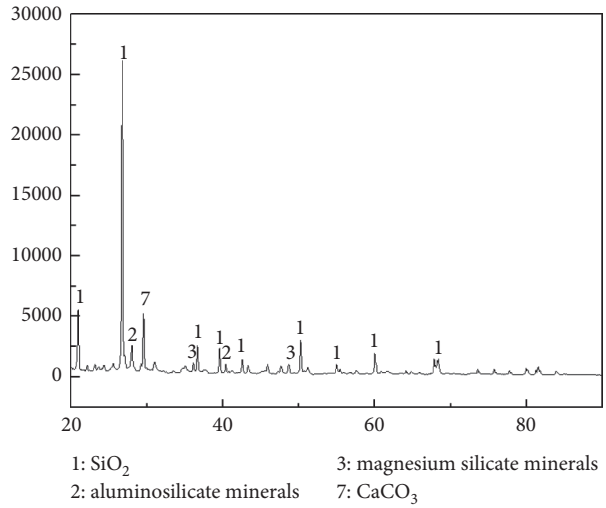

Figure 3: XRD patterns showing main mineral compositions of tailings.

performance (Table 3). While in use, the wave was fixed at the position of 150 mm above the base of the column. In addition, the maximum and the minimum cross-sectional diameters of the feed tank which is located on the ground are 50 cm and 30 cm, respectively, and the height of the tank is 40 cm; the flocculant holding tank with height of 20 cm and cross-sectional diameter of 15 cm was also located on the ground, and the settling column was mounted on a steel shelves; the ultrasonic equipment and the computer were sat on stools with 60 cm height, and the high-definition video camera was mounted on a small stand with the height of 80 cm; the pumps, shelves, and stools were all located on the ground.

2.3.2. Freeze-Drying Treatment and SEM Tests. Some studies have proved that freeze-drying could reduce structural changes [21, 22]. This process of drying and dewatering comprises a combination of vacuum technology and freezing technology and removes water via the sublimation of ice crystals in the sample.

The settling column was disassembled slightly at the end of the continuous thickening experiments (Figure 4(a)), and the samples were obtained from the bottom (Figure 4(b)). The sample holder is a hollow and thin-walled polyethylene plastic tube with 10 mm inner diameter and 100 mm length (Figure 4(c)). The sample holder was then transferred into the chamber of an LGJ-50C vacuum freeze-drying machine. The sample holder was frozen at -40°C for 6 h and maintained at a drying temperature of −10°C for 48 h. A vacuum of 50 mTorr was maintained throughout the freeze-drying cycle (Figure 4(d)).

The prepared samples were imaged by a Zeiss SEM normally operated at 20 kV voltage. In the SEM, micrographs from a selected suitable area of the freeze-drying samples were taken at magnifications around 2000×. The structure of flocs or aggregates in the SEM images was quantifiably analyzed using the software of Image *J*; then, the microstructural parameters of the SEM images including pore size and pore area were obtained. The steps to analyze the images using Image *J* were taken as follows:

(1) Open a SEM image in the software

(2) Click the "rectangular" button to select the area in the image

(3) Click the "image" button to convert the image to 8 bits image

(4) Adjust the threshold, and set the upper threshold level value "119" and the lower threshold value "0"

(5) Convert SEM image into binary images based on the threshold

(6) The parameters including pore size and pore area can be obtained using the function of "analyze articles"

Table 3: Ultrasonic frequency of experimental specimens.

No.	Frequency (kHz)	Rotation rate (rpm)
E1	16	4
E2	20	4
E3	22	4
E4	25	4
E5	28	4

3. Results and Discussion

3.1. The Changes of Bed Height. The bed height has a large impact on underflow concentration of thickeners; however, this research mainly focuses on the effect of ultrasonic frequency on the performance, and the values of bed height through the several experiments should be consistent with each other. Three experiments were performed at every frequency, and the average bed height profiles (Figure 5) are similar under the different ultrasonic frequencies. It can be seen that the bed heights are increased almost linearly with the increasing time in the noncontinuous condition; then, the bed heights are decreased with the increase in time from 60 minutes to 63 minutes since underflow was discharged in

(a) (b) (c) (d)

Figure 4: Process of pretreatment by the freeze-drying method. (a) Settling column. (b) Underflow sample. (c) Sample holder. (d) Vacuum freeze-drying machine.

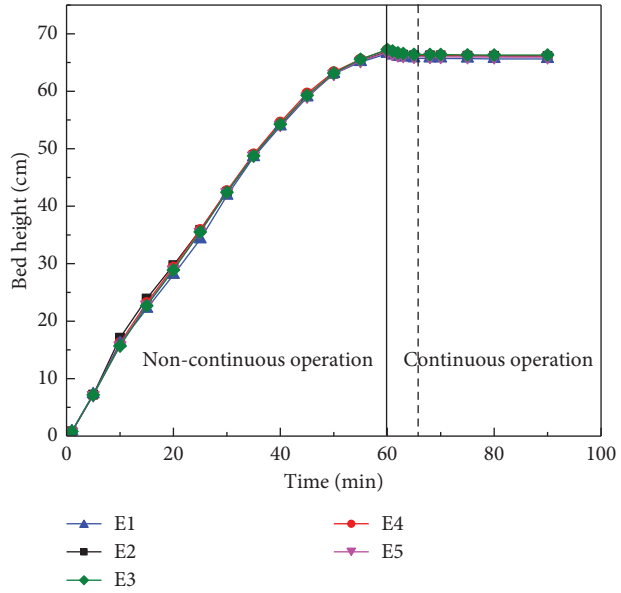

Figure 5: The average bed height changes with increasing time under different ultrasonic frequencies.

the continuous condition. Finally, the steady-state condition was maintained under circumstances of the underflow rate being from 0.092 L·min^{-1} to 0.094 L·min^{-1} and the feed rate being 0.6 L·min^{-1}. The average maximum and equilibrium bed heights under different ultrasonic frequencies are shown in Table 4.

The average rising rates of bed heights were calculated (Figure 6). In the first 60 minutes, the rising rates increased firstly with the time increasing and then decreased. The values of rising rates were more than 0 because of the continuous feeding and no discharging, and the maximum rate was obtained at the periods ranging from 5 minutes to 15 minutes. In continuous operation, the rising rates were dramatically decreased within the time ranging from 60 minutes to 63 minutes because of the underflow discharging; then, the rising rate of bed heights kept stable, which was around 0 cm/s. The average rising rates of bed heights essentially agree with each other under different ultrasonic frequencies, which means the ultrasonic frequency has little effect on the rising rate of bed height.

3.2. The Changes of Underflow Concentration. The underflow samples were obtained from the sampling point at different periods of 60 min, 61 min, 62 min, 65 min, 68 min, 70 min, 75 min, 80 min, and 90 min, respectively (Figure 7), and three underflow samples were taken to determine the concentration for each experiment. The average underflow concentration profiles (Figure 7) were similar for the different ultrasonic frequencies. The underflow concentrations rose at first and then kept stable in a higher level however, at the first 3 minutes, the concentrations were highly volatile. This is because the bed height is small at the initial stage, and the structure of underflow samples is relatively loose, and it was affected by rake rotation.

Table 4: The average maximum and equilibrium bed heights under different ultrasonic frequencies.

No.	Frequency (kHz)	The average maximum bed height (cm)	The equilibrium bed height (cm)
E1	16	68.6	67.4
E2	20	65.4	65.0
E3	22	65.8	65.0
E4	25	68.1	66.7
E5	28	67.6	66.9

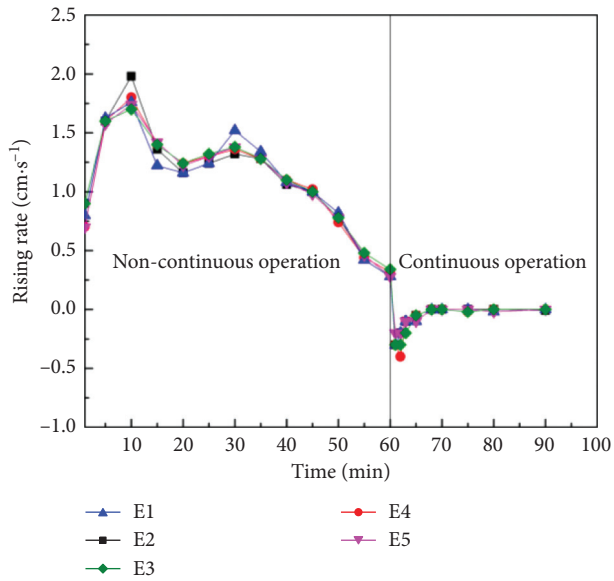

Figure 6: Average rising rate of bed height with increasing time under different ultrasonic frequencies.

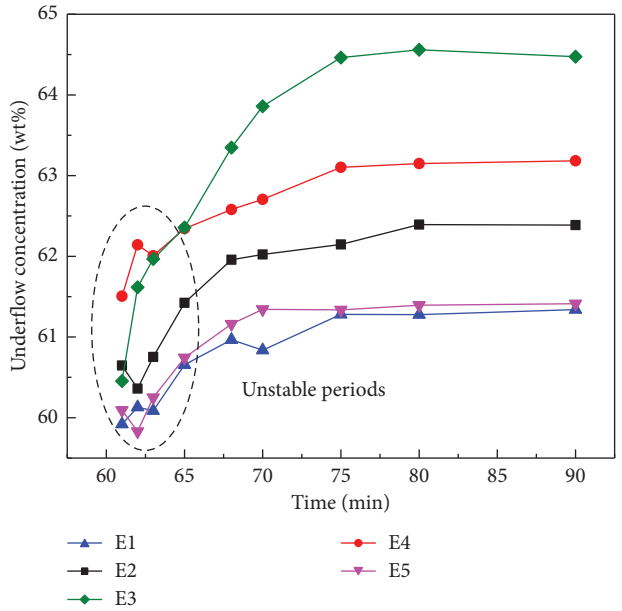

Figure 7: The changes of underflow concentration with increasing time under different ultrasonic frequencies.

The equilibrium data of underflow concentration was fitted to several types of equations using the software of origin. equation with a larger multiple correlation coefficient was fitted, which can be viewed as the optimal equation and the relationship between underflow concentration and time can be described using the equation as follows:

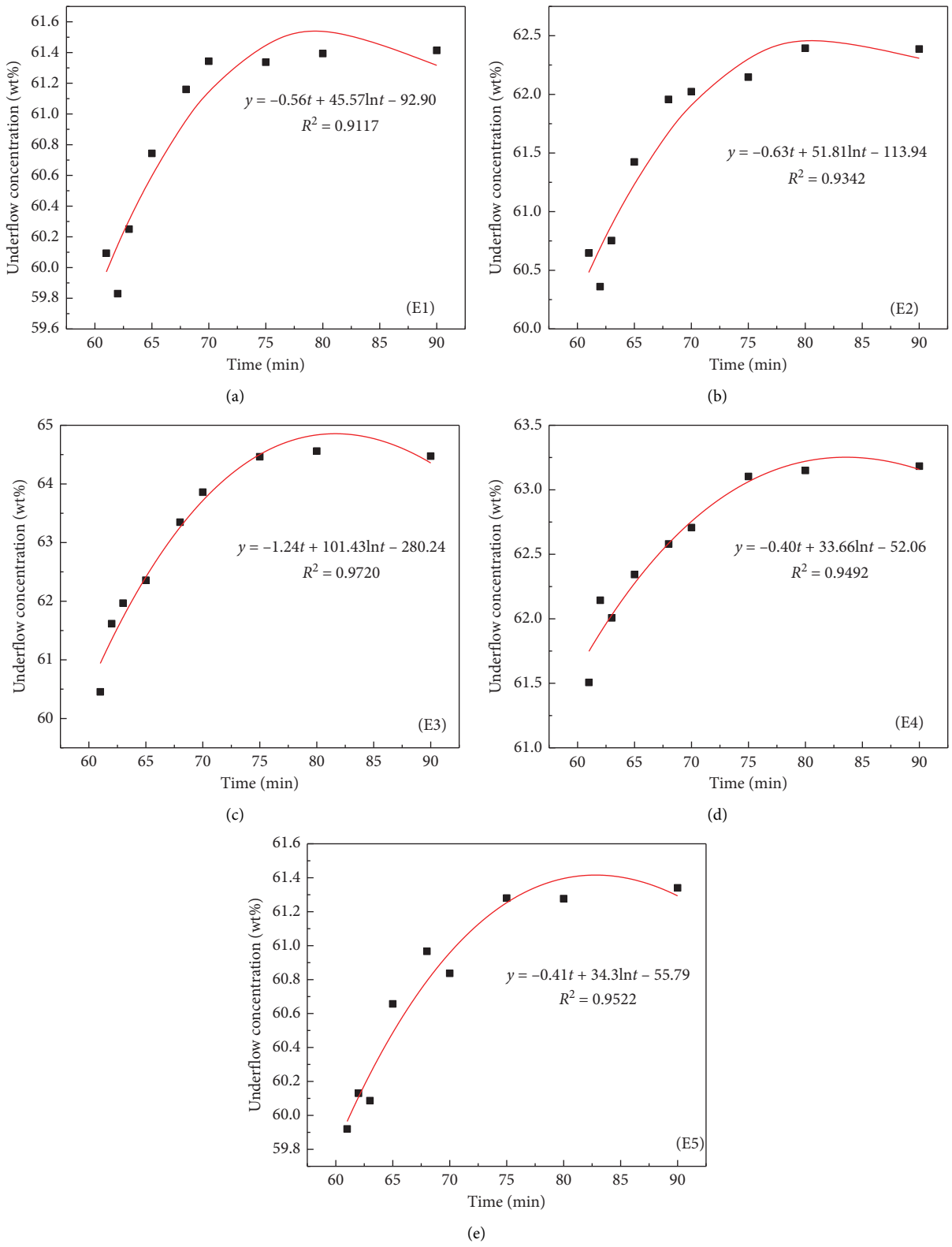

Figure 8: Evolution of the underflow concentration versus time under different ultrasonic frequencies. (a) 16 kHz. (b) 20 kHz. (c) 22 kHz. (d) 25 kHz. (e) 28 kHz.

Table 5: Underflow concentration under different ultrasonic frequencies.

No.	Ultrasonic frequency (kHz)	Underflow concentration (wt. %)
E1	16	61.34
E2	20	62.39
E3	22	64.47
E4	25	63.18
E5	28	61.41

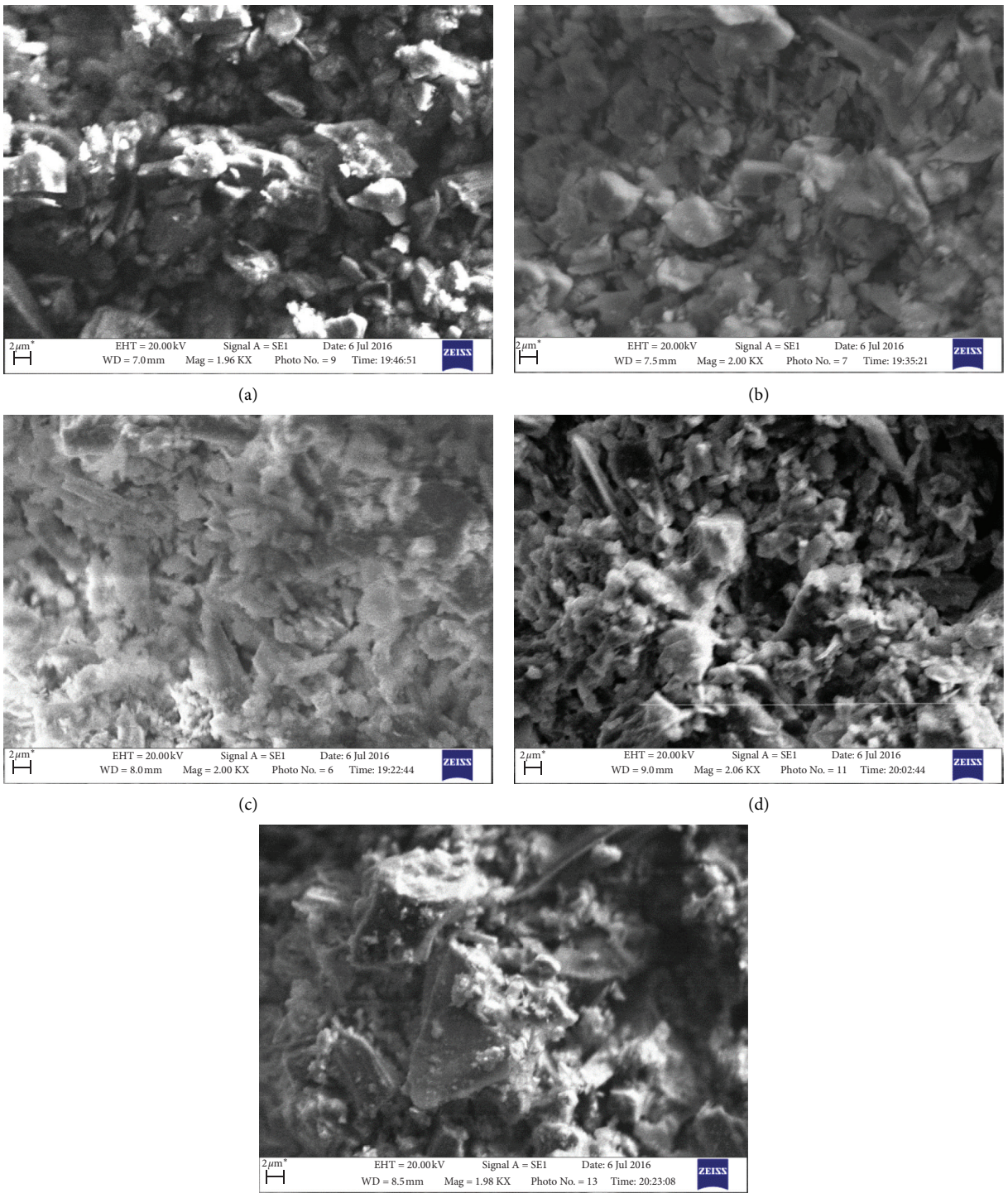

Figure 9: Microstructure of underflow samples under different ultrasonic frequencies. (a) 16 kHz. (b) 20 kHz. (c) 22 kHz. (d) 25 kHz. (e) 28 kHz.

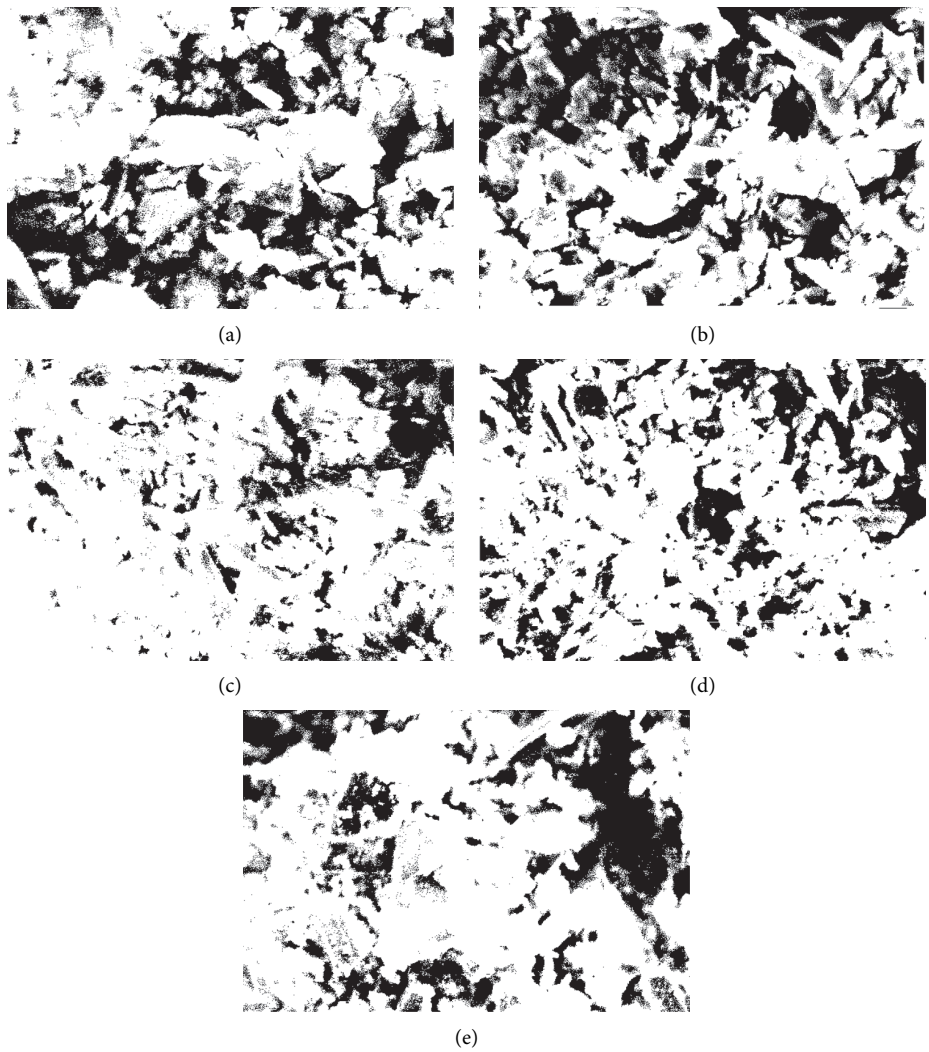

Figure 10: SEM binary image under different ultrasonic frequencies. (a) 16 kHz. (b) 20 kHz. (c) 22 kHz. (d) 25 kHz. (e) 28 kHz.

$$y = At + B \ln t + C, \tag{3}$$

where y represents underflow concentration (wt %), t represents run time (min), from 60 minutes to 90 minutes, and A, B, and C are fitting parameters.

The accuracy and variability of equation (3) were evaluated using the correlation coefficients R^2, which are shown in Figure 8. The maximum correlation coefficients R^2 (0.9720) were obtained at the ultrasonic frequency of 22 kHz, indicating that the actual underflow concentration is consistent with the fitted underflow concentration. The minimum correlation coefficient R^2 is 0.9117 when the ultrasonic frequency is 16 kHz, which indicated that the independent variable has a 91.17% chance of explaining the change in underflow concentration, and the model is quite correct. The values of the correlation coefficients R^2 are all higher than 0.91 that these models have enough accuracy to describe the relationship between underflow concentration and time.

The average steady-state underflow concentration under different ultrasonic frequencies is shown in Table 5. The underflow concentration increased firstly with the frequency increasing and then decreased. At the steady-state condition, the maximum underflow concentration (64.47 wt. %) was obtained at the ultrasonic frequency of 22 kHz, and the minimum value (61.34 wt. %) was obtained at the ultrasonic frequency of 16 kHz. In this study, the optimal thickening performance was obtained at the ultrasonic frequency of 22 kHz.

3.3. The Changes of Microstructure. It was found that the interaction and collision of small flocs and loose aggregates with each other form a network structure (Figure 9). The resolution of the microscopic images is 100 nm which has enough accuracy to observe the minimum size difference. These images show that the microstructures are quite different under different frequencies.

In order to quantify the network structure, the SEM images were converted into 8-bite images using the software of Image *J*; then, these images were converted into binary images (Figure 10) with adjusting the threshold as accurately as possible. The black area represents pores; conversely, the white area represents particles or aggregates; the pores and

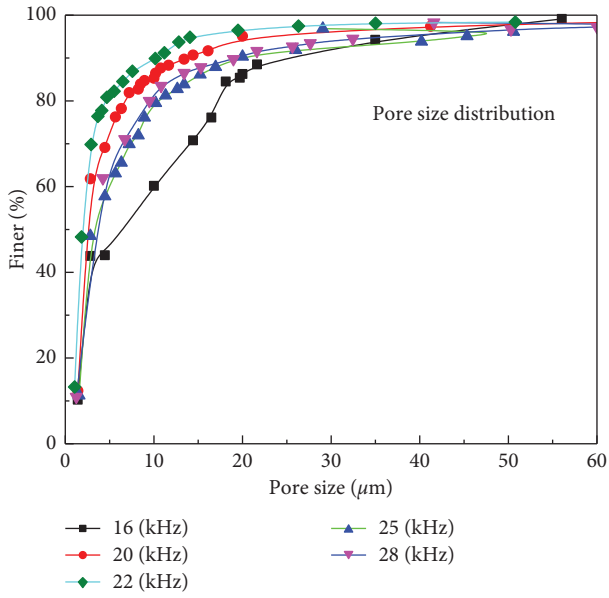

Figure 11: Distribution of pore size.

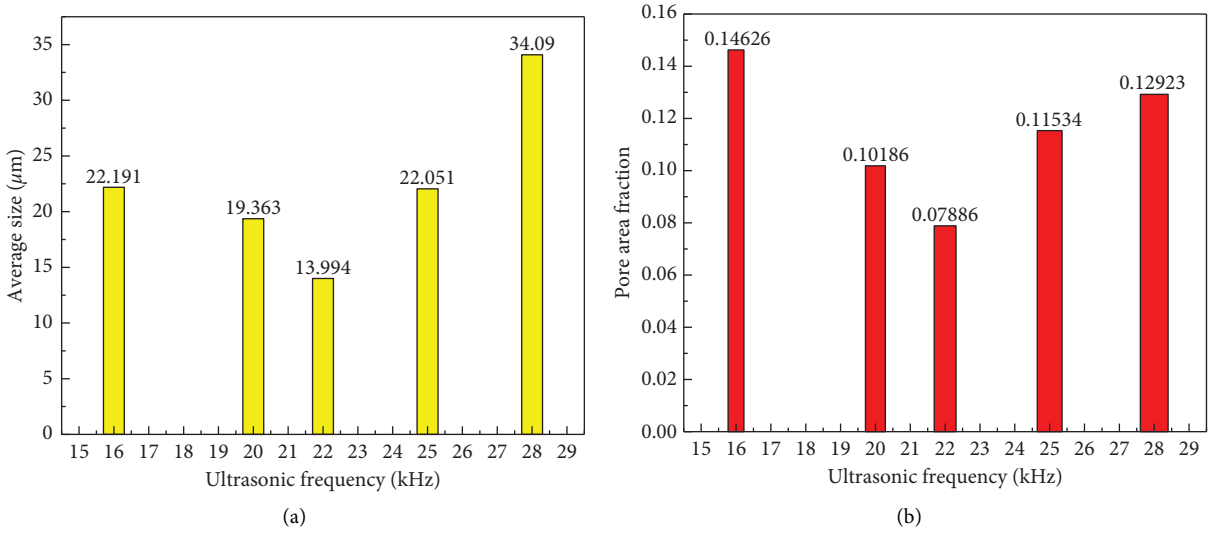

Figure 12: Microstructural parameters of underflow samples for different ultrasonic frequencies. (a) Pore average size. (b) Pore area fraction.

particles in the microstructure of the underflow samples can be clearly identified. The binary images were then used to analyze particles using Image *J* (analyze⟶analyze particles), and the data of pore size and pore area was obtained (Figure 11).

The pore size distribution is shown in Figure 11. These images show that the pore size increased firstly with the frequency increasing and then decreased overall, and the curve of the smallest pore size distribution was obtained when the ultrasonic frequency is 22 kHz. Increasing the ultrasonic frequency, which is less than 22 kHz, can decrease the sizes of pores; conversely, reducing the ultrasonic frequency can increase the sizes of pores when the ultrasonic frequency is more than 22 kHz, which is consistent with the change law of underflow concentration.

Figure 12 illustrates that the influences of ultrasonic frequency on the average size are significant. The average size of pore decreased firstly with frequency increasing and then decreased. The minimum average size of 13.994 μm was obtained at the ultrasonic frequency of 22 kHz, and the maximum value (34.09 μm) was obtained at the ultrasonic frequency of 28 kHz. Figure 12 shows that the variation law of pore area fraction is coincident with the average size of the pore with the ultrasonic frequency, and the minimum pore

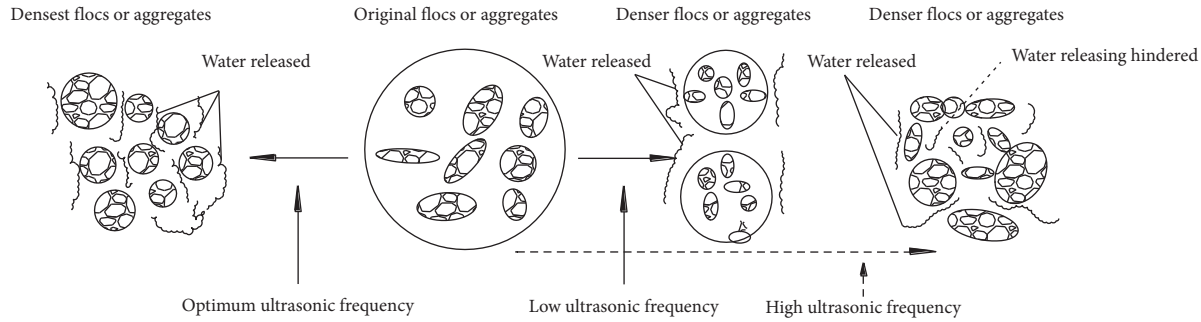

Figure 13: The changes of flocs or aggregate with the ultrasonic frequency.

fraction of 7.886% was obtained at the ultrasonic frequency of 22 kHz with the maximum value of 14.626% at an ultrasonic frequency of 16 kHz.

3.4. Mechanism of Ultrasonic Frequency on Flocs or Aggregates. Due to flocculant addition and raking, tailings particles can be flocculated and mixed to form a "honeycomb network" and relatively high density aggregates [23, 24], but there is still an amount of water trapped in aggregates. Based on the above, the ultrasonic frequency has a significant influence on flocs' microstructure which has a large impact on underflow concentration in the process of thickening. The shock wave generated by the cavitation of the ultrasonic wave can lead to a fierce collision between flocs or aggregates; then, a part of the trapped water was released, and new denser flocs or aggregates formed. When the ultrasonic frequency is less than optimal frequency, the water released much and the aggregate was denser with the increasing frequency; then, the higher underflow concentration can be produced with decreasing pore sizes and areas. However, while the ultrasonic frequency attains some extent, the energy of the shock wave is so large to hinder water releasing effectively from the broken flocs or aggregates; then, the pore sizes and areas increase compared to the circumstance of the optimum ultrasonic frequency. The changes of flocs or aggregate with the ultrasonic frequency are shown in Figure 13.

4. Conclusions

The study results allow us to draw the following conclusions:

(1) The focus of this study is on the application of the different ultrasonic frequencies on thickening performance in continuous tests which is different from the traditional work in batch tests. The ultrasonic frequency has a nonsignificant influence on the rising rate of bed height, but a significant influence on underflow concentration.

(2) The underflow concentration increases firstly with increasing ultrasonic frequency and then decreases. The maximum underflow concentration of 64.47 wt. % is obtained at the ultrasonic frequency of 22 kHz, and the difference is 3.13 wt. % between the minimum and maximum values.

(3) The present study proposes a linear logarithmic function that can determine the underflow concentration with run time at a certain ultrasonic frequency. The minimum correlation coefficient R^2 of the equations is 0.9117, implying that the model is relatively reliable.

(4) Based on SEM images analysis, the minimum pore average size (13.994 μm) and pore average fraction (7.886%) of underflow samples are obtained when the ultrasonic frequency is 22 kHz, implying that 22 kHz is the optimum ultrasonic frequency combining results of the underflow concentration.

In future research works, the authors will consider applying the results obtained from this lab testing to a deep cone thickener with diameter of 14 m. We also demonstrate the results of the indoor research based on the technical problems that may arise during the thickening process. To further investigate ultrasonic frequency on thickener performance, more research could be conducted on the mathematical model of tailings thickening under ultrasonic irradiation.

Data Availability

The data used to support the findings of this study are available from the corresponding author upon request.

Conflicts of Interest

The authors declare that there are no conflicts of interest regarding the publication of this paper.

Acknowledgments

This work was financially supported by the National Natural Science Foundation of China (52004152) and Project ZR2020QE100 supported by Shandong Provincial Natural Science Foundation.

References

[1] J. I. Langlois and A. Cipriano, "Dynamic modeling and simulation of tailing thickener units for the development of control strategies," *Minerals Engineering*, vol. 131, no. 1, pp. 131–139, 2019.

[2] L. Orejarena and M. Fall, "Mechanical response of a mine composite material to extreme heat," *Bulletin of Engineering Geology and the Environment*, vol. 67, no. 3, pp. 387–396, 2008.

[3] M. Benzaazoua, M. Fall, and T. Belem, "A contribution to understanding the hardening process of cemented pastefill," *Minerals Engineering*, vol. 17, no. 2, pp. 141–152, 2004.

[4] A. Kesimal, B. Ercikdi, and E. Yilmaz, "The effect of desliming by sedimentation on paste backfill performance," *Minerals Engineering*, vol. 16, no. 10, pp. 1009–1011, 2003.

[5] C. Qi and A. Fourie, "Cemented paste backfill for mineral tailings management: review and future perspectives," *Minerals Engineering*, vol. 144, no. 10, p. 1, 2019.

[6] S. P. Usher, R. Spehar, and P. J. Scales, "Theoretical analysis of aggregate densification: impact on thickener performance," *Chemical Engineering Journal*, vol. 151, no. 1, p. 202, 2009.

[7] H. Jiao, A. Wu, H. Wang, S. Zhong, R. Ruan, and S. Yin, "The solids concentration distribution in the deep cone thickener: a pilot scale test," *Korean Journal of Chemical Engineering*, vol. 30, no. 2, pp. 262–268, 2013.

[8] A. T. Owen, P. D. Fawell, and J. D. Swift, "The preparation and ageing of acrylamide/acrylate copolymer flocculant solutions," *International Journal of Mineral Processing*, vol. 84, no. 1, p. 3, 2007.

[9] R. Arjmand, M. Massinaei, and A. Behnamfard, "Improving flocculation and dewatering performance of iron tailings thickeners," *Journal of Water. Process Engineering*, vol. 31, no. 1, p. 1, 2019.

[10] R. Spehar, A. Kiviti-Manor, P. Fawell, S. P. Usher, M. Rudman, and P. J. Scales, "Aggregate densification in the thickening of flocculated suspensions in an un-networked bed," *Chemical Engineering and Science*, vol. 122, p. 585, 2014.

[11] B. R. Gladman, M. Rudman, and P. J. Scales, "The effect of shear on gravity thickening: pilot scale modelling," *Chemical Engineering Science*, vol. 65, no. 14, pp. 4293–4301, 2010.

[12] B. B. G. van Deventer, S. P. Usher, A. Kumar, M. Rudman, and P. J. Scales, "Aggregate densification and batch settling," *Chemical Engineering Journal*, vol. 171, no. 1, pp. 141–151, 2011.

[13] P. Grassia, Y. Zhang, A. D. Martin et al., "Effects of aggregate densification upon thickening of Kynchian suspensions," *Chemical Engineering Science*, vol. 111, no. 111, pp. 56–72, 2014.

[14] J. Du, R. Mcloughlin, and R. S. C. Smart, "Improving thickener bed density by ultrasonic treatment," *International Journal of Mineral Processing*, vol. 133, pp. 91–96, 2014.

[15] G. Önal, M. Özer, and F. Arslan, "Sedimentation of clay in ultrasonic medium," *Minerals Engineering*, vol. 16, no. 2, pp. 129–134, 2003.

[16] B. Liu, Y. T. Gao, A. B. Jin, and X. Wang, "Dynamic characteristics of superfine tailings–blast furnace slag backfill featuring filling surface," *Construction and Building Materials*, vol. 242, p. 2, 2020.

[17] W. Sun, A. X. Wu, and H. J. Wang, "The change laws of flow characteristics of backfill paste mixed by unclassified tailings and waste rock," *Rock and Soil Mechanics*, vol. 4, p. 3464, 2013.

[18] A. X. Wu, W. Sun, and H. J. Wang, "Experiment research on shear behavior of subsidence backfill body mixed by unclassified tailings and waste rocks," *Chinese Journal of Rock Mechanics and Engineering*, vol. 32, no. 5, p. 917, 2013.

[19] P. Xing, Y. X. Xiang, H. J. Wang, F. L. Zhou, S. Y. Wang, and Y. S. Chu, "Research on flocs selection of tailings with high sliming in baishitamu copper mine," *Modern Mining*, vol. 563, p. 49, 2016.

[20] W. H. Gao, H. J. Wang, H. Chen, L. H. Yang, and L. Zhang, "Study on main factors of underflow concentration in the dynamics thickening process of tailings," *Metal Mine*, vol. 485, p. 102, 2016.

[21] M. Cassanelli, I. Norton, and T. Mills, "Role of gellan gum microstructure in freeze drying and rehydration mechanisms," *Food Hydrocolloids*, vol. 75, pp. 51–61, 2018.

[22] G. Straller and G. Lee, "Shrinkage of spray-freeze-dried microparticles of pure protein for ballistic injection by manipulation of freeze-drying cycle," *International Journal of Pharmaceutics*, vol. 532, no. 1, pp. 444–449, 2017.

[23] J. Du, R. A. Pushkarova, R. S. C. Smart, and C. Smart, "A cryo-SEM study of aggregate and floc structure changes during clay settling and raking processes," *International Journal of Mineral Processing*, vol. 93, no. 1, pp. 66–72, 2009.

[24] D.-l. Wang, Q.-l. Zhang, Q.-s. Chen, C.-c. Qi, Y. Feng, and C.-c. Xiao, "Temperature variation characteristics in flocculation settlement of tailings and its mechanism," *International Journal of Minerals, Metallurgy and Materials*, vol. 27, no. 11, pp. 1438–1448, 2020.